Numerical simulation of solitary wave propagation over a steady current

Jisheng Zhang[1], Jinhai Zheng[2], Dong-Sheng Jeng[3] and Yakun Guo[4]

ABSTRACT

A two-dimensional numerical model is developed to study the propagation of a solitary wave in the presence of a steady current flow. The numerical model is based on the Reynolds-averaged Navier-Stokes (RANS) equations with a k-ε turbulence closure scheme and an internal wave-maker method. To capture the air-water interface, the volume of fluid (VOF) method is used in the numerical simulation. The current flow is initialized by imposing a steady inlet velocity on one computational domain end and a constant pressure outlet on the other end. The desired wave is generated by an internal wave-maker. The propagation of a solitary wave travelling with a following/opposing current is simulated. The effects of the current velocity on the solitary wave motion are investigated. The results show that the solitary wave has a smaller wave height, larger wave width and higher travelling speed after interacting with a following current. Contrariwise, the solitary wave becomes higher with a smaller wave width and lower travelling speed with an opposing current. The regression equations for predicting the wave height, wave width and travelling speed of the resulting solitary wave are for practical engineering applications. The impacts of current flow on the induced velocity and the turbulent kinetic energy (TKE) of a solitary wave are also investigated.

Keywords: Wave-current interaction, solitary wave, RANS model, numerical simulation

[1]Professor, State Key Laboratory of Hydrology-Water Resources and Hydraulic Engineering, Hohai University, Nanjing 210098, China

[2]Professor, State Key Laboratory of Hydrology-Water Resources and Hydraulic Engineering, Hohai University, Nanjing 210098, China

[3]Professor, Griffith School of Engineering, Griffith University Gold Coast Campus, QLD 4222, Australia

[4]Reader, School of Engineering, University of Aberdeen, Aberdeen, AB24 3UE, UK

INTRODUCTION

In many studies, solitary waves have been used to model the behaviour of the leading wave of storm surges (Hsiao et al., 2008; Lara et al., 2011; Wu & Hsiao 2013), and the propagation process is acknowledged as a critical problem in evaluating the effects produced by storm surges in coastal areas. In the early stage of a storm surge event, the water level is usually rising and currents are formed along the coast. Sea waves, which are normally generated in the deep ocean, are riding on the currents and travelling toward the shore (wave following current); whereas when the storm surge departs, currents change direction and move seaward (wave opposing current) (Xiao et al., 2013). Nonlinear interactions between the leading wave of the storm surge (solitary-like wave) and the ambient current can redistribute the energy of an incident wave in time and space, creating an inundated scale (Kowalik et al., 2006).

The mechanics of wave-current interaction has been widely investigated by analytical approximation methods (Madsen, 1994; Groeneweg and Klopman, 1998; Hsu et al., 2009; Zhang et al., 2011) and laboratory experiments (Kemp and Simons, 1982, 1983; Mathisen and Madsen, 1996; Fredsöe et al., 1999; Umeyama, 2009, 2011) in the past decades. Recently, numerical models based on the Navier-Stokes (NS) equations have been developed for the prediction of wave-current interactions. For example, Park et al. (2001) developed a numerical wave tank with a finite-difference scheme, the mark-and-cell method and the subgrid-scale (SGS) turbulence model for modelling the nonlinear wave-current-body interaction. In their model, a wave-maker is established at the inflow boundary by prescribing the inflow velocities, while the current field is gradually introduced in the entire fluid region. Li et al. (2007) presented a NS solver using a finite-volume scheme, the volume of fluid (VOF) method and the SGS turbulence model for the interactions between breaking waves and the current over a cut-cell grid. In the case of waves following the current, an external

generator combining the inflow motions of the waves and the current is applied at the inflow boundary. In the case of waves in an opposing current, an internal generator is used to describe the opposing current, by adding source functions in the mass and the momentum equations.

Although many efforts have been made to understand the mechanics of wave-current interactions, all of the aforementioned studies have focused solely on the interaction between the current and the regular or the irregular wave. To date, investigations of the solitary wave-current interactions are limited. In this study, a Reynolds-averaged Navier-Stokes (RANS) solver using a finite-volume scheme, the VOF method and the k-ε turbulence model is developed to model a solitary wave propagating over a following/opposing current. The steady current in the computational domain is achieved by imposing a uniform velocity inflow boundary and a pressure outflow boundary and the desired waves are generated by incorporating a source function into the mass conservation equation. Because experiments on solitary wave-current interaction are not currently available, the model is validated by laboratory measurements of linear wave-current interactions (Umeyama 2005, 2011). The model is then applied to investigate the effects of current velocity on the mechanics of solitary wave-current interactions and on the resulting wave height, wave width, wave speed, velocity and turbulent kinetic energy (TKE).

GOVERNING EQUATIONS

The RANS equations are used to describe the incompressible fluid motion resulting from wave-current interaction as follows.

$$\frac{\partial \langle u_i \rangle}{\partial x_i} = 0 \tag{1}$$

$$\frac{\partial \rho \langle u_i \rangle}{\partial t} + \frac{\partial \rho \langle u_i \rangle \langle u_j \rangle}{\partial x_j} = -\frac{\partial \langle p \rangle}{\partial x_i} + \frac{\partial}{\partial x_i}\left[\mu\left(\frac{\partial \langle u_i \rangle}{\partial x_j} + \frac{\partial \langle u_j \rangle}{\partial x_i}\right)\right] + \frac{\partial}{\partial x_i}\left(-\rho \langle u_i' u_j' \rangle\right) + \rho g_i \tag{2}$$

where x_i is the Cartesian coordinate, $\langle u_i \rangle$ is the ensemble mean velocity component, t is time, ρ is the fluid density, $\langle p \rangle$ is the fluid pressure, μ is the dynamic viscosity, and g is the gravitational acceleration. The Reynolds stress term, $-\rho\langle u_i' u_j' \rangle$, is modelled using the k-ε turbulence model. Applying the eddy-viscosity assumption, the Reynolds stress term is modelled as follows (Launder and Spalding, 1974; Rodi, 1993):

$$-\rho\langle u_i' u_j' \rangle = \mu_t \left(\frac{\partial \langle u_i \rangle}{\partial x_j} + \frac{\partial \langle u_j \rangle}{\partial x_i} \right) - \frac{2}{3}\rho\delta_{ij}k \tag{3}$$

where μ_t is the turbulent viscosity, k is the turbulent kinetic energy (TKE) and δ_{ij} is the Kronecker delta. Based on Equation (3), Equation (2) is rewritten as follows:

$$\frac{\partial \rho\langle u_i \rangle}{\partial t} + \frac{\partial \rho\langle u_i \rangle\langle u_j \rangle}{\partial x_j} = -\frac{\partial}{\partial x_i}\left[\langle p \rangle + \frac{2}{3}\rho k\right] + \frac{\partial}{\partial x_i}\left[\mu_{eff}\left(\frac{\partial \langle u_i \rangle}{\partial x_j} + \frac{\partial \langle u_j \rangle}{\partial x_i}\right)\right] + \rho g_i \tag{4}$$

where $\mu_{eff}=\mu+\mu_t$ is the total effective viscosity.

The most commonly used equations for the k-ε turbulence model are as follows:

$$\frac{\partial \rho k}{\partial t} + \frac{\partial \rho\langle u_j \rangle k}{\partial x_j} = \frac{\partial}{\partial x_j}\left[\left(\mu + \frac{\mu_t}{\sigma_k}\right)\frac{\partial k}{\partial x_j}\right] + \rho P_k - \rho\varepsilon \tag{5}$$

$$\frac{\partial \rho\varepsilon}{\partial t} + \frac{\partial \rho\langle u_j \rangle\varepsilon}{\partial x_j} = \frac{\partial}{\partial x_j}\left[\left(\mu + \frac{\mu_t}{\sigma_\epsilon}\right)\frac{\partial \varepsilon}{\partial x_j}\right] + \frac{\varepsilon}{k}\left(C_{1\varepsilon}\rho P_k - C_{2\varepsilon}\rho\varepsilon\right) \tag{6}$$

$$\mu_t = \rho C_\mu \frac{k^2}{\varepsilon} \tag{7}$$

This model employs values for the constants that are calibrated by comprehensive data fitting for a wide range of turbulent flows (Rodi, 1993), i.e., C_μ= 0.09, σ_k=1.00, σ_ε= 1.30, $C_{1\varepsilon}$= 1.44 and $C_{2\varepsilon}$= 1.92. The standard k-ε turbulence model is only valid for fully developed flow, and the near-wall model, which utilizes the log-law, is required at the first grid point above the bottom wall.

As discussed by Lin & Liu (1999), Ha et al. (2013) and Zhang et al. (2014), the waves generated by the source function do not interact with the waves reflected from inside the

domain or with the ambient current, and such an influence (which is a limitation of the wave absorbing/generating boundary) can be avoided by using an internal wave maker. In this study, to generate the desired wave, the internal wave-maker method developed by Lin and Liu (1999) is adopted to avoid the simultaneous specification of wave and current at the inflow boundary. In the source region, a source function $S(x_i, t)$ is added to the mass conservation equation (Equation (1)) as follows:

$$\frac{\partial \langle u_i \rangle}{\partial x_i} = S(x_i, t) \quad in\ \Omega \tag{8}$$

where $S(x_i, t) \neq 0$ within the source region Ω. The value of $S(x_i, t)$ depends on the wave characteristics, and its formulation for a solitary wave is as follows:

$$S(x_i, t) = \frac{CH}{A}\text{sech}^2\left[\sqrt{\frac{3H}{4d^3}}(4d/\sqrt{H/d} - Ct)\right] \tag{9}$$

where C is the wave phase velocity, H is the wave height, A is the area of the source region, and d is the still water depth. In this study, the area (denoted as A) of the source region in which the wave-maker is acting is predefined and remains constant during the simulation. As recommend by Lin (2008), the source region has a height that is 10% of the water depth (0.65d-0.75d) and a width that is 5% of the wavelength.

NUMERICAL METHODS

The entire computational domain is divided into a structured mesh, and the RANS governing equations are solved using a two-step projection method with a finite volume discretization (Bussmann et al., 2002; Ferziger and Peric, 2002). In this model, the fluid variables, such as the pressure and the velocities, are defined at the cell centroids. To convert cell centroid data to the face centroid to evaluate the gradient of the quantity at the cell centroid, the least square linear reconstruction method developed by Barth (1992) is applied. The forward time difference method is used for the discretization of the time derivative. The two-phase VOF

method of Hirt and Nichols (1981) is used to track the water-air interface. The idea behind VOF is to define a function F to represent the fractional volume of water in the fluid. The piecewise linear interface calculation method of Rider and Kothe (1998) is used to reconstruct the air-water interface in the cells with values of $0<F<1$.

The boundary conditions must be specified to solve the governing equations (see Figure 1). A uniform inflow velocity is given at the left-hand-side boundary for the generation of a steady current flow, while a pressure outlet (a hydrostatic pressure distribution) is defined at the right-hand-side boundary. Sponge layers with widths of two wavelengths to damp the vertical velocity of the current are defined near two sides of the computational domain. Therefore, the wave motion becomes negligible at the inlet and the outlet boundaries. After a steady current flow is established in the domain, the internal wave-maker is activated to generate the desired waves within the computational domain. The waves propagating to the left-hand-side (upstream) are opposing the steady current and the waves travelling to the right-hand-side (downstream) are following the steady current. Zero surface tension, i.e., $\frac{\partial k}{\partial n} = \frac{\partial \varepsilon}{\partial n} = 0$, is assumed at the air-water interface. A no-slip boundary using the wall function is set for the bottom boundary condition. That is the boundary conditions for the momentum equations are based on the bottom stress estimated from the log-law. The dimensionless wall-unit ($y^+=u_* y/\nu$, where u_* is the friction velocity, y is the distance between the first grid point and the bottom wall and ν is the kinematic viscosity) indicates that the distance between the first grid point and the bottom wall is in the range of 22-32 in the study; therefore, the log-law for bottom boundary condition is valid for the simulation. To obtain computational stability, the time interval (Δt) is automatically adjusted at each time step to satisfy the Courant-Friedrichs-Levy condition and the diffusive limit condition (Liu et al., 1999).

RESULTS AND DISCUSSION

Model validation of linear wave-current interactions

Because there are no existing laboratory experiments of solitary wave-current interactions, the well-documented laboratory measurements of wave following/opposing a steady current by Umeyama (2005, 2011) are used for the model validation of this RANS model. Umeyama (2005, 2011) carried out a series of experiments in a wave channel 25m long, 0.7m wide and 1.0m deep. In Umeyama's tests (2011), the water depth and wave period were fixed at d=0.3 m and T=1.0 s, respectively. Tests W1 and W2 were for waves without the presence of a following current with wave heights of 0.0103 m and 0.0234 m, respectively. Tests WC1 and WC2 were the waves of W1 and W2 superimposed on a following current with a depth-averaged velocity of u_0=0.08 m/s. The time-dependent water surface and horizontal velocity were measured. As the mean-current profiles are not provided by Umeyama (2011), the laboratory measurements of the mean-current profile in Umeyama (2005) with a water depth of d=0.2 m, a wave period of T=1.2 s and a depth-averaged velocity of u_0=0.12 m/s are used for the comparison.

To validate the proposed numerical model with the laboratory tests, a computational domain with a range of -20 m <x<20 m and 0 m < y< 0.34 m is used. In the horizontal direction, the cells are uniformly distributed with Δx=0.004 m. In the vertical direction, Δy=0.0004 m is used in the water-air interface region to accurately capture the water wave profile and Δy=0.004 m is applied in the near-wall and other regions to avoid excessive computational expense. In the case of the wave-current interaction, the computational domain is initialized by a water body with a set water depth (d=0.3 m for Umeyama (2011) and d=0.2 m for Umeyama (2005)) and a set horizontal velocity (u_0=0.08 m/s for Umeyama (2011) and u_0=0.12 m/s for Umeyama (2005)), with the goal of rapidly reaching a steady current flow

before the generation of the desired wave. In both simulations, the RANS model was run 25 wave periods (i.e., 25 seconds), and the numerical results averaged from the last 5 wave periods are compared with the laboratory experiments.

Comparisons of the simulated with the measured water surface profiles (Umeyama, 2011) for both the wave-alone and the wave-current cases are presented in Figure 2. The results show that the water surface profile resulting from the wave-current interaction is different from the wave-alone surface profile. The wave length increases after interacting with the following current, which is primarily from the Doppler shift (the impact of a steady current on the intrinsic wave frequency) (Wolf and Prandle, 1999). When the waves follow with a steady current, the wave height is reduced. This phenomenon is caused by wave action conservation (defined as wave energy divided by intrinsic angular frequency). As the wave length increases and wave height decreases, the wave steepness decreases. The simulated differences of wave height between W1-WC1 and W2-WC2 are 0.0018 m and 0.0042 m, respectively. Greater wave steepness leads to a larger reduction in wave height. Comparisons of simulated and measured horizontal-velocity profiles (Umeyama, 2011) for the wave-alone and wave-current cases are shown in Figures 3 and 4, respectively. The results also indicate that the propagation of a surface wave can significantly affect the profile of the induced horizontal velocity. When the current flow meets the wave trough, the current speed above the bottom boundary layer decreases toward the free water surface (see the velocity distribution at t=0.00 s in Figure 4). When the wave crest arrives, the current velocity increases significantly (see the velocity distribution at t=0.50 s in Figure 4).

The mean current profiles for three different cases (current without wave, current following wave, and current opposing wave) are also validated. In the case of the current without the

wave, the simulated mean current profiles are compared with the logarithmic equation, in which the velocity distributions are calculated from $U/u_* = u_* y/\nu[1-y/(2d)]$ in the viscous sublayer and the formula of Umeyama and Gerritsen (1992) in the turbulent layer (see Figure 5). Figure 6 shows the comparison of the simulated and the measured mean current profiles when a wave coexists with a following/opposing current (Umeyama, 2005). The comparison shown in Figure 6(a) reveals that the primary effects of introducing a following wave are an increase in the mean velocity in the turbulent boundary layer near the bottom wall and a decrease in the mean velocity in the upper layer, indicating that the boundary layer thickness is reduced. The results in Figure 6(b) shows that the mean velocities in the upper flow increase in the current direction, suggesting that the wave-induced mass transport is enhanced by the current. The results also show that the turbulence intensities are increased by the presence of the waves, which can be modelled by introducing an apparent bed roughness (larger than the physical bottom roughness). Generally speaking, the numerical results agree well with the laboratory measurements.

Model application for solitary wave-current interaction

In the real ocean, the solitary wave rides on the current, and the energy of the incident wave may be redistributed from the wave-current interaction (Kowalik et al., 2006). The primary concern is whether these two waves can be linearly superposed for the purpose of determining the resulting sea surface height and travelling speed. This validated RANS model is applied to numerically investigate the propagation of a solitary wave over a steady current. In the example, the water depth d=20.0 m and two different wave heights are tested (H=4.0 m and H=3.0 m). The current velocity is varied from -3.0 m/s to 3.0 m/s with an equal interval of 0.5 m/s. A slip boundary condition (zero shear stress) is adopted for the bottom wall, and a fully uniform current flow is achieved before the generation of the solitary waves. To avoid the

effect of the grid size on the simulation, grid refinement is applied. The grid near the water surface is refined until no noticeable changes in the solution are achieved. The final mesh used for the simulation is Δx=0.1 m and Δy=0.025 m. In the numerical study, the effects of the (uniformly-distributed) current velocity on the water surface profile, the travelling speed and the TKE of the resulting solitary wave are analyzed.

Effect of the current velocity on wave height

The wave height of a solitary wave is one of the key factors affecting the wave-induced inundation area in coastal regions. Figure 7 shows the effects of the current flow on the water surface profile at dimensionless time $t/[g(d+H)]^{0.5}$=60 (in which H is the solitary wave height without the current). The wave height increases with an opposing current flow, while it decreases with a following current. The induced wave heights of a solitary wave (h) are 4.74 m, 4.00 m and 3.36 m for the cases with an opposing current (u_0=-3.0 m/s), no current (u_0=0.0 m/s) and a following current (u_0=3.0 m/s), respectively, when H=4.0 m. The change of wave height (0.74 m, 18.5% of height of current-free solitary wave) induced by the opposing current is slightly larger than the change (0.64 m, 16.0% of height of current-free solitary wave) induced by the following current. More numerical experiments with a broad range of current velocities were run to investigate the effect of current velocity on solitary wave height. Figure 8 shows the effect of current velocity on the solitary wave height for the cases of H=4.0 m and H=3.0 m. Carrying out the regression analysis on the data in Figure 8 yields the following:

$h/H=-0.1514u_0/(gH^2/d)^{0.5}+1.0072$ with R^2=0.9970 for the case of H=4.0 m (10)

$h/H=-0.9342u_0/(gH^2/d)^{0.5}+1.0079$ with R^2=0.9979 for the case of H=3.0 m (11)

The results indicate that the impact of the flow current on the induced solitary wave height becomes stronger when the solitary wave has a greater height. Meanwhile, Equations (10) &

(11) may be used to roughly estimate the wave height of the resulting solitary wave for the purpose of practical engineering applications.

Effect of the current velocity on the width of the wave

Because the total volume of a solitary wave remains constant, the surface profile (in terms of the wave width) therefore changes as the wave height changes. In this study, a characteristic wave width (w) is defined as the distance between two cross-points where the horizontal line y=20.05 m meets the surface outline of the solitary wave. As illustrated in Figure 9, where w_0 is the width of the wave without a current, the wave width is greatly affected by the steady current. The wave is elongated when the solitary wave is superposed with a following current and it is shortened when encountering an opposing current. With the same current speed, the impact of an opposing current on the wave width is more significant than that of a following current. For example, in the case of a solitary wave with H=4.0 m, the wave width is reduced by approximately 6.9% in the case of u_0=-3.0 m/s and it is increased by approximately 17% in the case of u_0=3 m/s. The linear relation between the current speed and the wave width of the induced solitary wave (w) is as follows:

$w/w_0=0.1199u_0/(gH^2/d)^{0.5}+0.9712$ with $R^2=0.9730$ for the case of H=4.0 m (12)

$w/w_0=0.0939u_0/(gH^2/d)^{0.5}+0.9856$ with $R^2=0.9917$ for the case of H=3.0 m (13)

These results show that the influence of the current on the wave width is slightly weaker as the wave height of the solitary wave changes from H=4.0 m to H=3.0 m.

Effect of the current velocity on the wave travelling speed

The travelling speed of a solitary wave (determined by the time-dependent position of the wave crest) is also affected by the ambient current flow (see Figure 10 where the dotted line is the linear superposition of the wave phase velocity and the current speed). The data in Figure

10(a) show that the induced velocity is approximately 18.10 m/s (117.9% of the phase velocity of the current-free solitary wave) in the case with a following current (u_0=3.0 m/s), and it is approximately 12.41 m/s (80.8% of the phase velocity of a current-free solitary wave) in the case with an opposing current (u_0=-3.0 m/s). The travelling speed of the resulting solitary wave can be estimated by the following formula:

$u/[g(d+H)]^{0.5}=0.9456u_0/[g(d+H)]^{0.5}+0.9940$ with $R^2=0.9998$ for the case of H=4.0 m (14)

$u/[g(d+H)]^{0.5}=0.9629u_0/[g(d+H)]^{0.5}+1.0010$ with $R^2=0.9998$ for the case of H=3.0 m (15)

As indicated in Figure 10, the resulting velocity is obtained by the linear superposition of the wave phase velocity and the current speed when the wave opposes the current. However, the error caused by the linear assumption can no longer be neglected when the wave follows a high-speed current. It is also expected that the linear superposition of the wave phase velocity and the current speed is not suitable for the prediction of the travelling speed of the resulting solitary wave when the speed of the opposing current is increased sufficiently.

Effect of the current velocity on the ensemble-averaged velocity

After interacting with the steady current, the ensemble-averaged velocity of a solitary wave may change significantly (see Figures 11 & 12 for the case with H=4.0 m at the dimensionless time $t/[g(d+H)]^{0.5}$=60). The data in Figures 11(b) & 12(b) show that when a solitary wave travels by itself, only the region around the wave crest has a strong ensemble-averaged velocity with a maximum magnitude of 2.5-3.0 m/s. The wave front is moving forward and upward, while the lee side of the wave crest is travelling forward and downward. When travelling with a following current (u_0=3.0 m/s), the solitary wave retains a similar ensemble-averaged velocity field with an increased intensity (see Figure 11(a)). The data in Figure 12(a) show that the highest speed occurs in the wave crest, with a magnitude of 5.0-5.5 m/s. However, the data in Figure 11(c) show that the velocity field is significantly modified

when a solitary wave travels (from right to left) against a steady flow (u_0=-3.0 m/s, from left to right). The induced wave crest is still travelling from right (downstream) to left (upstream), but its moving speed is greatly reduced to a magnitude of 0-0.5 m/s (see Figure 12(c)).

Effect of the current velocity on the turbulent kinetic energy (TKE)

The TKE is defined as the mean kinetic energy per unit mass associated with eddies in the turbulent flow, and in the RANS equations it is quantified by the mean of the turbulent normal stresses. The TKE is usually produced by fluid shear, friction or buoyancy, and is transferred down the turbulence energy cascade. The dissipation of TKE is primarily from the viscous forces at the Kolmogorov scale. The data in Figure 13 show the effect of the current velocity on the distribution of the TKE in a solitary wave. The turbulence level is extremely low when a solitary wave travels without an ambient current flow, and the TKE is nearly zero (see Figure 13(b)). The data in Figures 13(a) and 13(c) show that the existence of a following/opposing current slightly increase the TKE (in the range of 0.001-0.002 m^2/s^2). The vertical line shown in Figures 13 (a) and 13(c) is the contour line for TKE=0.001 m^2/s^2. The TKE is significantly increased in the case of a solitary wave interacting with the ambient current flow around marine structures or in the shoaling region, and this RANS model with k-ε turbulence closure provides a valuable basis to investigate this type of problem. The results from the mesh refinement show that unrealistically intense TKE may be induced near the water surface by numerical noise and the independency of numerical solutions on grid size must be ensured in the simulation.

CONCLUSIONS

A RANS model is used to simulate the solitary wave propagation over a following/opposing steady current. Good agreement between the numerical simulation and Umeyama's laboratory

measurements (Umeyama 2005, 2011) show that the model is able to predict wave-current interactions. The calibrated model was applied to investigate the effects of current velocity on the dynamics of the solitary wave-current interaction and its induced wave height, wave width, travelling speed, velocity and TKE. The following conclusions are based on the numerical results.

(1) A solitary wave with a following current has a smaller wave height, longer wave width and higher travelling speed. After interacting with an opposing current, the solitary wave is higher, shorter and slower. For practical engineering applications, regression equations for predicting the wave height, wave width and travelling speed of the resulting solitary wave are provided.

(2) When travelling with a following current, the solitary wave retains a similar ensemble-averaged velocity field with an increased intensity. However, the velocity field is significantly modified when the solitary wave travels against a steady flow. The induced wave crest is still travelling against the current flow, but speed of motion is reduced.

(3) The existence of a following/opposing current flow slightly increases the turbulence level; the TKE is in the range of 0.001-0.002 m^2/s^2. This RANS model with k-ε turbulence closure provides a valuable basis for investigating a solitary wave interacting with ambient current flow around marine structures or in the shoaling region, where the TKE may be significantly increased.

ACKNOWLEDGEMENTS

The authors are grateful for support from the National Natural Science Foundation of China Grant #51209083, #51137002 and #41176073, the Natural Science Foundation of Jiangsu Province (China) Grant #BK2011026, the 111 Project under Grant No. B12032, the Fundamental Research Funds for the Central University, China (2013B31614), and the Carnegie Trust for Scottish Universities. The authors are grateful for the constructive comments made by reviewers, which significantly improved the quality of the final manuscript.

REFERENCES

Barth, T.J. (1992). "Aspects of unstructured grids and finite-volume solvers for the Euler and Navier-Stokes equations." In AGARD, Special Course on Unstructured Grid Methods for Advection Dominated Flows.

Bussmann, M., Kothe, D.B., Sicilian, J.M. (2002). "Modeling high density ratio incompressible interfacial flows." ASME 2002 Joint U.S.-European Fluids Engineering Division Conference.

Ferziger, J.H., Peric, M. (2002). "Computational methods for fluid dynamics". Springer-Verlag.

Fredsöe, J., Andersen, K.H., Sumer, B.M. (1999). "Wave plus current over a ripple-covered bed." Coastal Engineering, 38, 177-221.

Groeneweg, J., Klopman, G. (1998). "Changes of the mean velocity profiles in the combined wave-current motion described in a GLM formulation." Journal of Fluid Mechanics, 370, 271-296.

Ha, T., Lin, P., Cho, Y.-S. (2013). "Generation of 3D regular and irregular waves using Navier-Stokes equations model with an internal wave maker." Coastal Engineering, 76, 55-67.

Hsiao, S.C., Hsu T.W., Lin T.C., Chang, Y.H. (2008). "On the evolution and run-up of breaking solitary waves on a mild sloping beach." Coastal Engineering, 55 (12), 975-988.

Hsu, H.C., Chen, Y.Y., Hsu, J.R.C., Tseng, W.J. (2009). "Nonlinear water waves on uniform current in Lagrangian coordinates." Journal of Nonlinear Mathematical Physics, 16, 47-61.

Kemp, P.H. and Simons, R.R. (1982). "The interaction of waves and a turbulent current: waves propagating with the current." Journal of Fluid Mechanics, 116, 227-250.

Kemp, P.H., Simons, R.R. (1983). "The interaction of waves and a turbulent current: waves propagating against the current." Journal of Fluid Mechanics, 130, 73-89.

Kowalik, Z., Proshutinsky, T., Proshutinsky, A. (2006). "Tide-tsunami interactions." Science of Tsunami Harzards, 24, 4.

Lara, J. L., Losada, I. J., Maza, M., Guanche, R. (2011). "Breaking solitary wave evolution over a porous underwater step." Coastal Engineering, 58, 837-850.

Launder, B.E., Spalding, D.B. (1974). "The numerical computation of turbulence flows." Computer Methods in Applied Mechanics and Engineering, 3, 269-289.

Li, T., Troch, P., Rouck, J.D. (2007). "Interactions of breaking waves with a current over cut cells." Journal of Computational Physics, 223, 865-897.

Lin, P. (2008). "Numerical modelling of water waves". Taylor & Francis.

Lin, P., Liu, P. L.-F. (1999). "Internal wave-maker for Navier-Stokes equations models." Journal of Waterway, Port, Coastal, and Ocean Engineering, ASCE, 125(4), 207-415.

Liu, P. L.-F., Lin, P., Chang, K.A., Sakakiyama, T. (1999). "Numerical modelling of wave interaction with porous structures." Journal of Waterway, Port, Coastal and Ocean Engineering, ASCE, 125(6), 322-330.

Madsen, O.S. (1994). "Spectral wave-current bottom boundary layer flows." Proceedings of the 24th International Conference on Coastal Engineering.

Mathisen, P.P.,Madsen, O.S. (1996). “Waves and currents over a fixed rippled bed: I, bottom roughness experienced by waves in the presence and absence of currents.” Journal of Geophysical Research, 101, 16533-16542.

Park, J.C., Kim, M.H., Miyata, H. (2001). “Three-dimensional numerical wave tank simulations on fully nonlinear wave-current-body interactions.” Journal of Marine Science and Technology, 6, 70-82.

Rider, W.J.,Kothe, D.B. (1998). “Reconstructing volume tracking.” Journal of Computational Physics, 141, 112-152.

Rodi, W. (1993). “Turbulence Models and their Application in Hydraulics-State-of-The-Art Review.” IAHR Publication.

Umeyama, M. (2005). “Reynolds stresses and velocity distributions in a wave-current coexisting environment.” Journal of Waterway, Port, Coastal, and Ocean Engineering, 131(5), 203-212.

Umeyama, M. (2009). “Changes in turbulent flow structure under combined wave-current motions.” Journal of Waterway, Port, Coastal and Ocean Engineering, 135, 213-227.

Umeyama, M. (2011). “Coupled PIV and PTV measurements of particle velocities and trajectories for surface waves following a steady current.” Journal of Waterway, Port, Coastal and Ocean Engineering, 137, 85-94.

Umeyama, M., Gerritsen, F. (1992). “Velocity distribution in uniform sediment-laden flow”. Journal of Hydraulic Engineering, 118(2), 229-245.

Wolf, J., Prandle, D. (1999). “Some observations of wave-current interaction.” Coastal Engineering, 37, 471-485.

Wu, T.Y., Hsiao, S.C. (2013). “Propagation of solitary waves over a submerged permeable breakwater.” Coastal Engineering, 81, 1-18.

Xiao, H., Huang, W., Tao, J., Liu, C. (2013). “Numerical modeling of wave-current forces acting on horizontal cylinder of marine structures by VOF method.” Ocean Engineering, 67, 58-67.

Zhang C., Zheng, J., Wang, Y., Zeki, D. (2011). “Modeling wave-current bottom boundary layers beneath shoaling and breaking waves.” Geo Marine Letter, 31(3): 189-201.

Zhang J., Zhang, Y., Jeng, D., Liu, P. L.-F., Zhang, C. (2014). “Numerical simulation of wave-current interaction using a RANS solver.” Ocean Engineering, 75, 157-164.

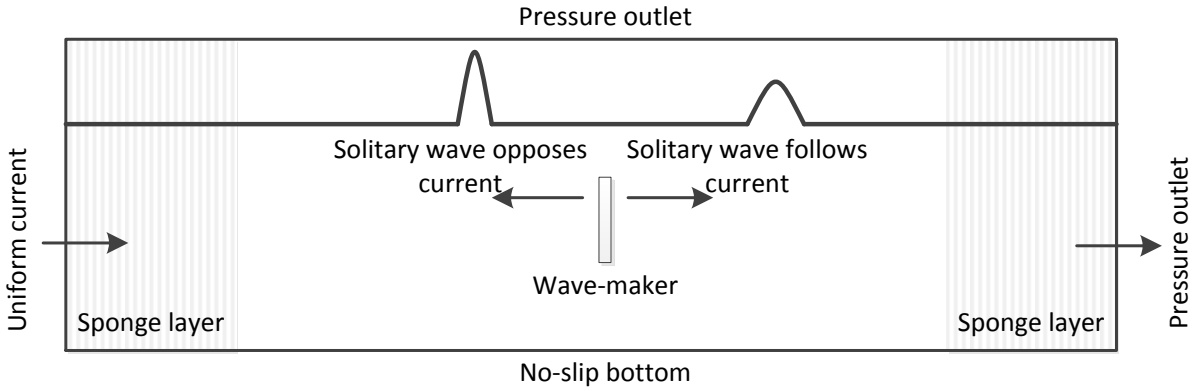

Figure 1 Sketch of the computational domain and boundary conditions for modelling wave-current interaction

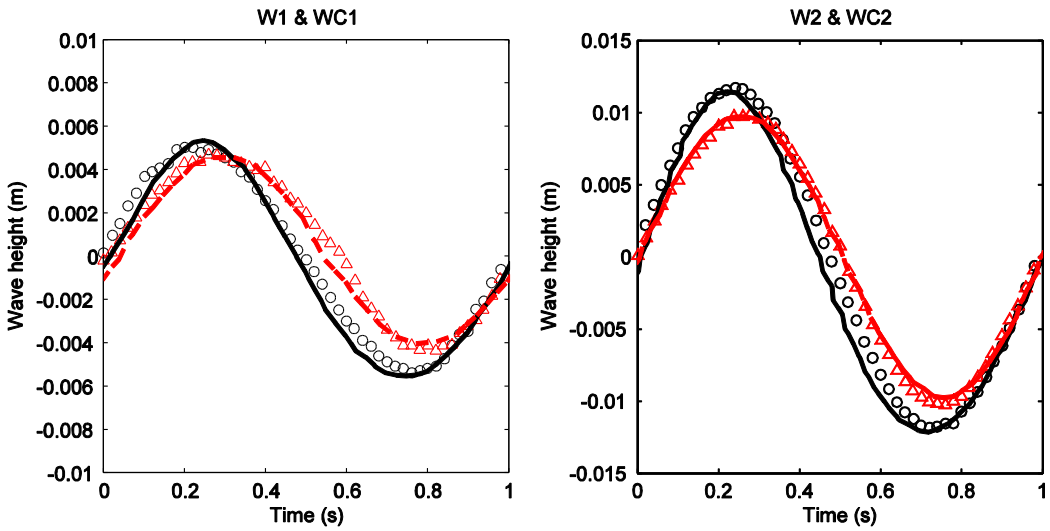

Figure 2 Comparison of the simulated and measured water surface profile in both wave-alone and wave-current cases. ○: wave-alone measurement; Δ: wave-current measurement; ─: wave-alone simulation; ─: wave-current simulation

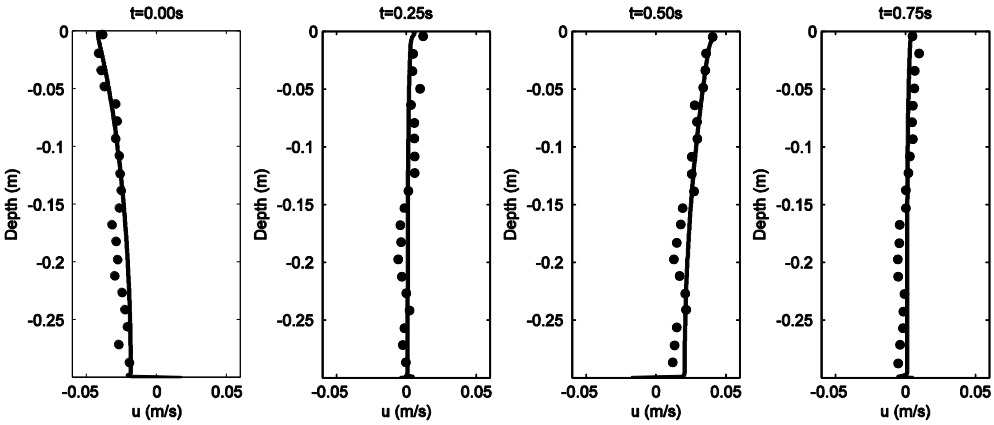
t=0.00s
t=0.25s
t=0.50s
t=0.75s
Depth (m)
u (m/s)
0
-0.05
-0.1
-0.15
-0.2
-0.25
-0.05
0
0.05

(a) W1

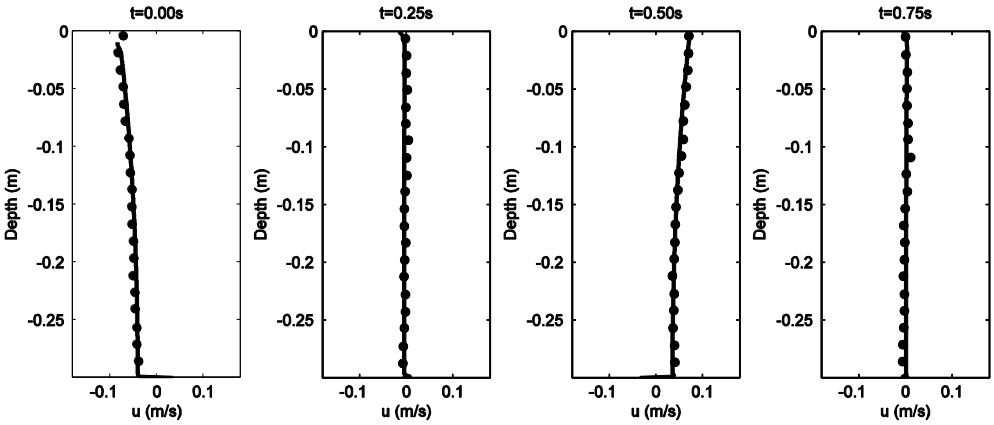

(b) W2

Figure 3 Comparison of the simulated and measured horizontal-velocity profiles for wave-alone cases.●: measurement; ─: simulation

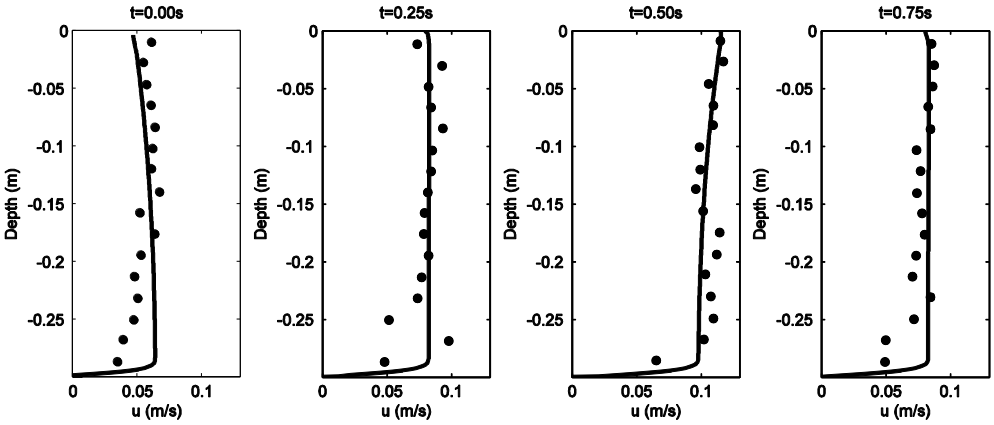

(a) WC1

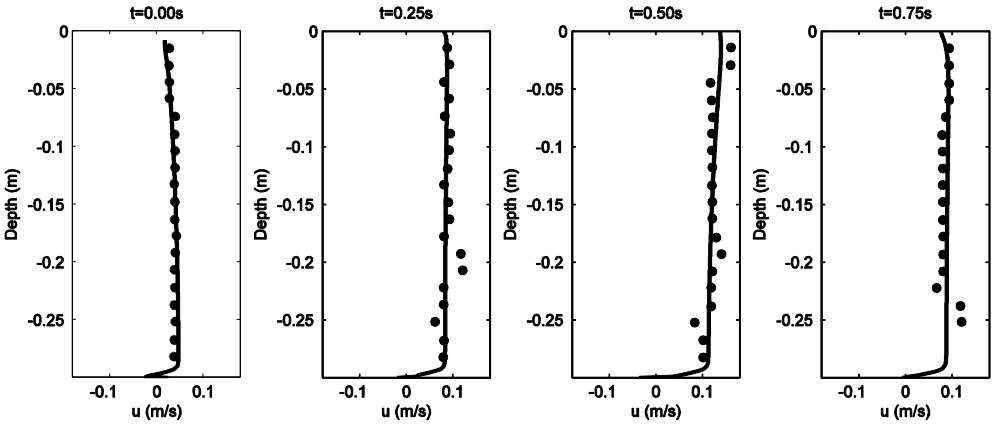

(b) WC2

Figure 4 Comparison of the simulated and measured horizontal-velocity profiles for wave-current cases.●: measurement; ─: simulation

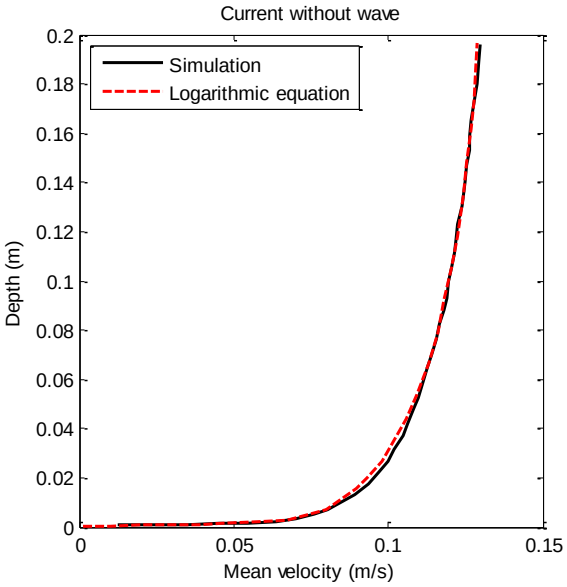

Figure 5 Comparison of the simulated and measured mean current profiles for current without wave

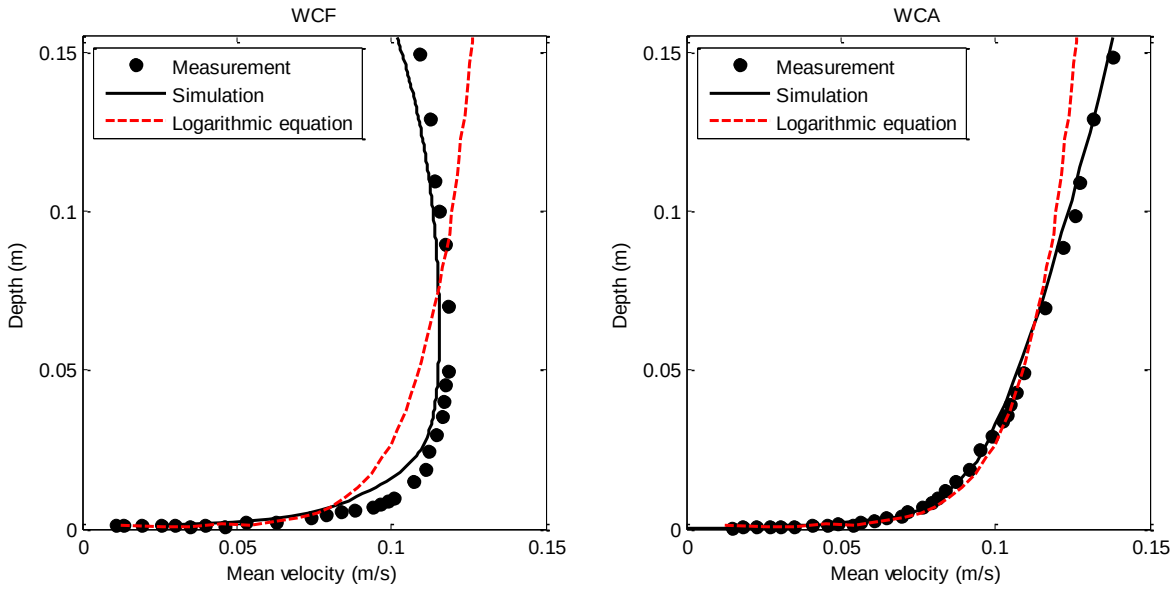

(a) (b)

Figure 6 Comparison of the measured, simulated and theoretical calculated mean current profiles: (a) wave following current; (b) wave opposing current

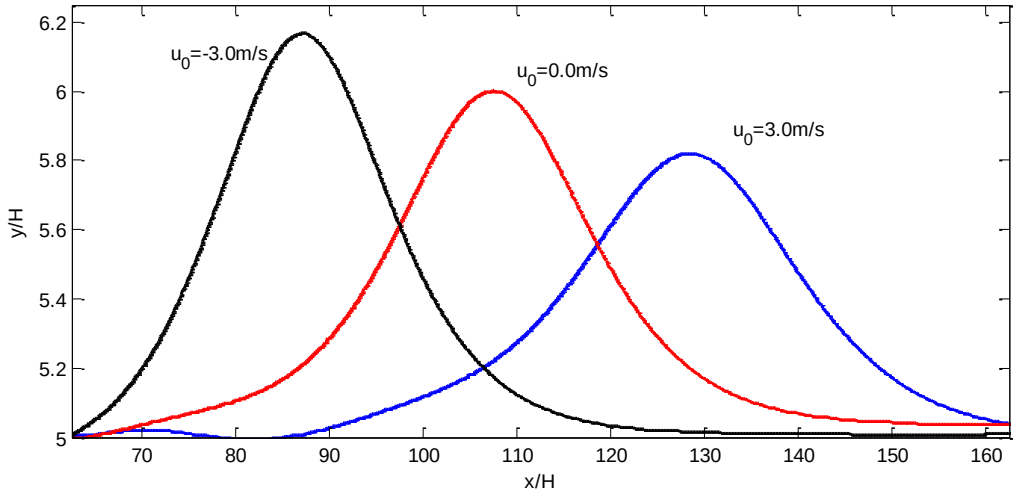

Figure 7 Effect of the current velocity on the water surface profile of solitary wave. ─: u_0=-3.0 m/s; ─: u_0=0.0m/s; ─: u_0=3.0 m/s

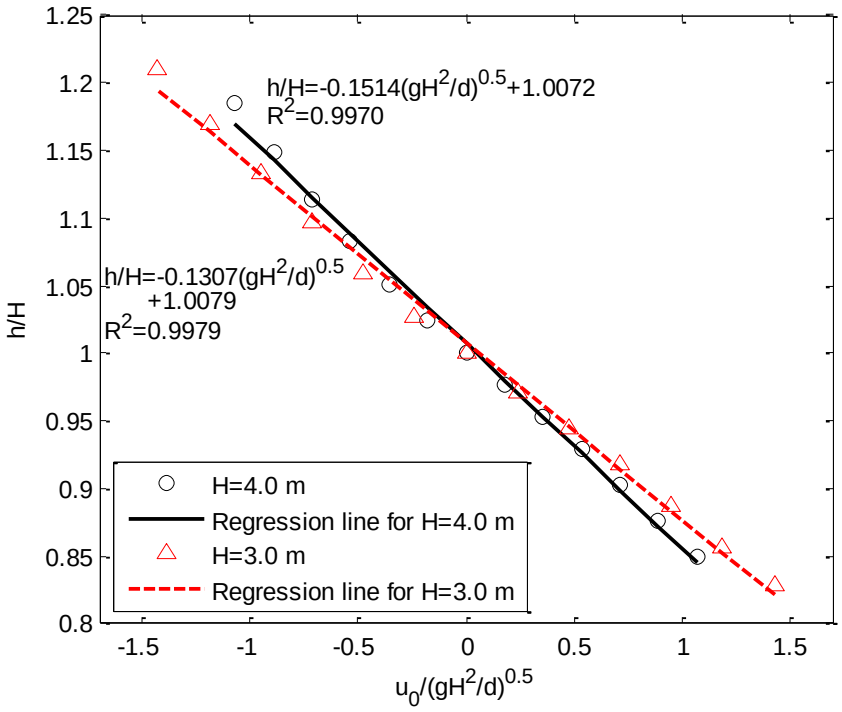

Figure 8 Effect of the current velocity on the wave height of solitary wave

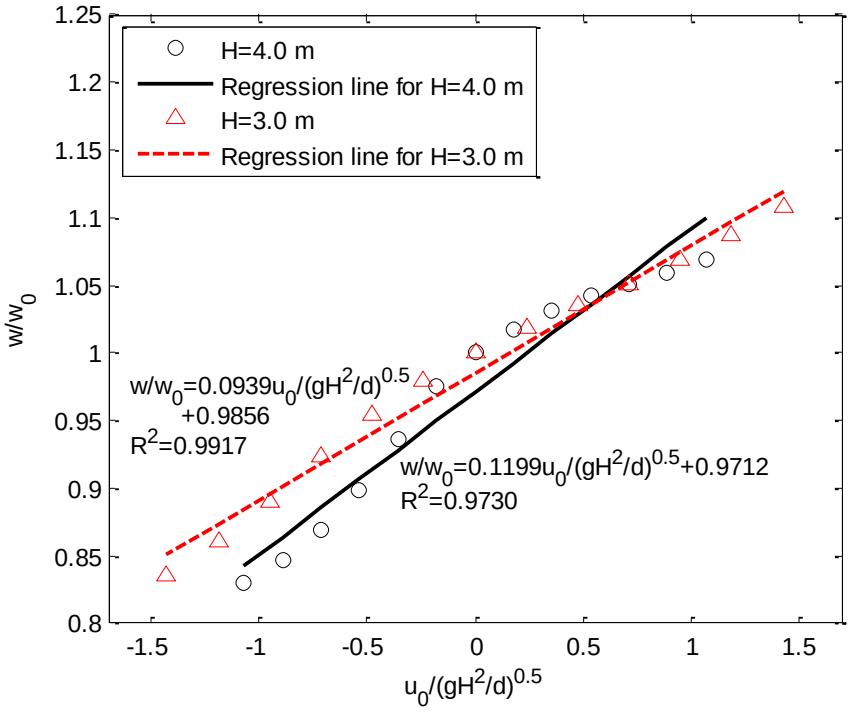

Figure 9 Effect of the current velocity on the wave width of solitary wave

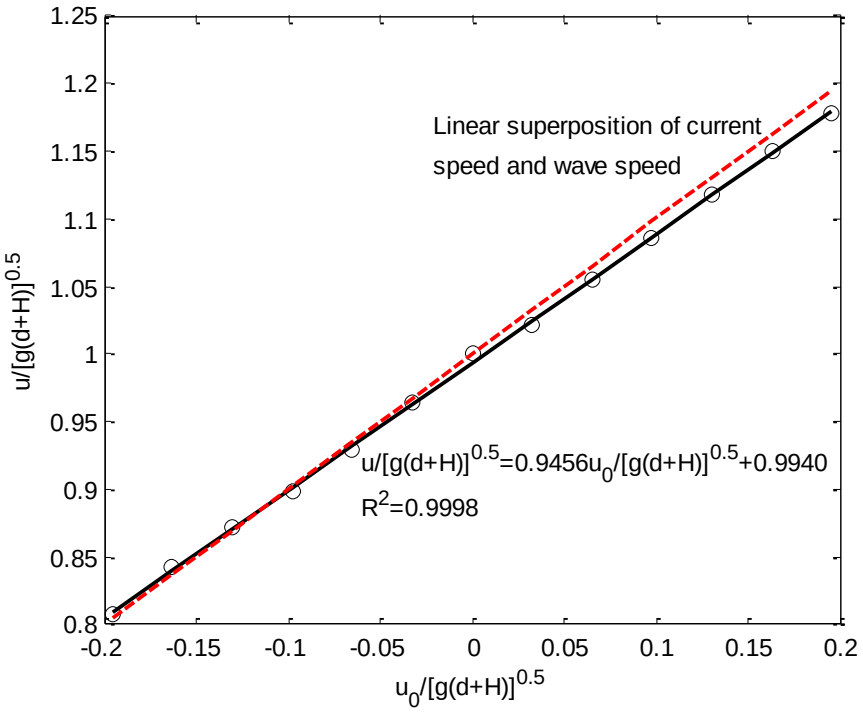

(a) H=4.0 m

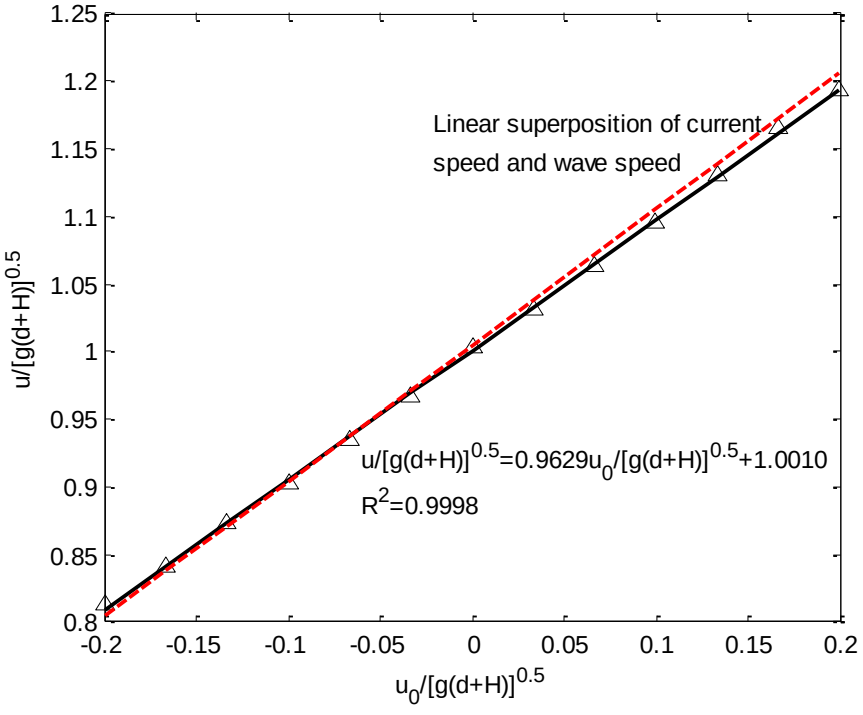

(b) H=3.0 m

Figure 10 Effect of the current velocity on the travelling speed of solitary wave. --: linear regression line; - -: linear superposition of current speed and wave speed

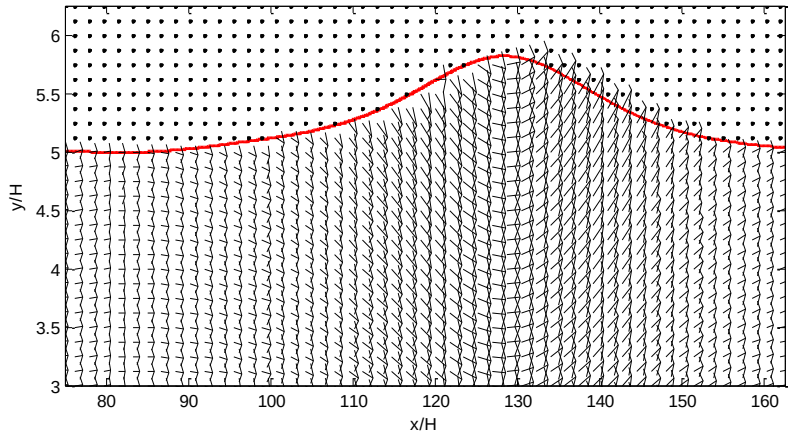

(a) u_0=3.0 m/s

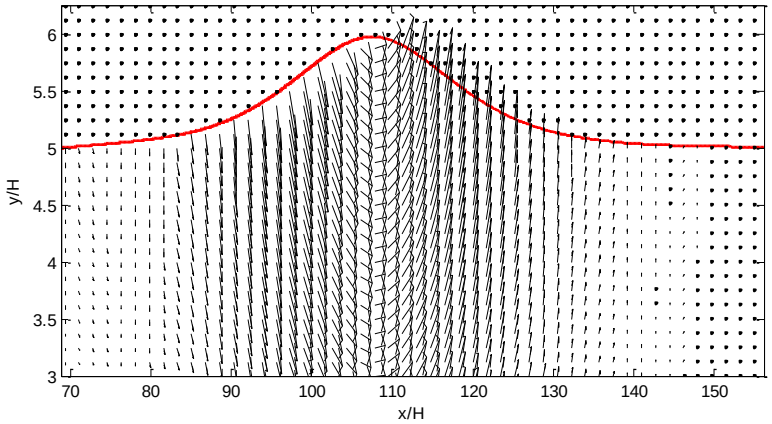

(b) u_0=0.0 m/s

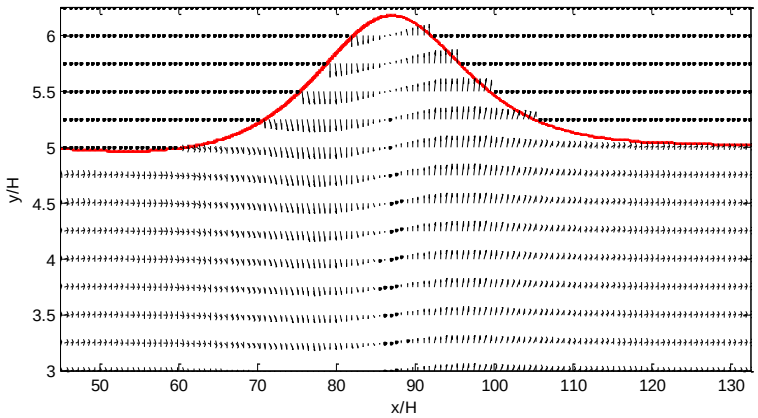

(c) u_0=-3.0 m/s

Figure 11 Effect of the current velocity on the ensemble-averaged velocity field

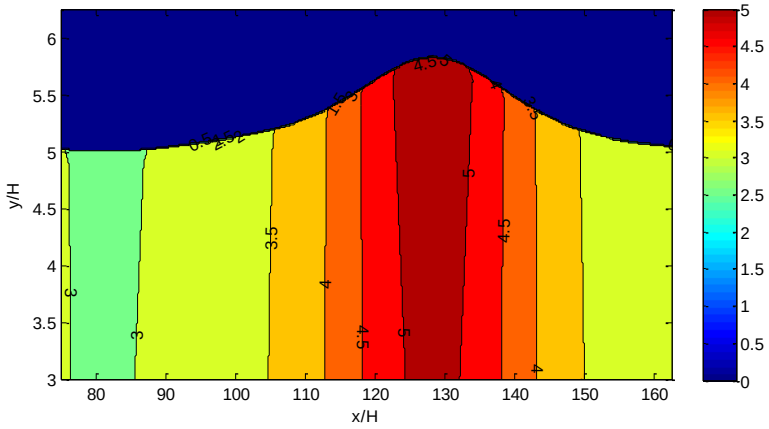

(a) u_0=3.0 m/s

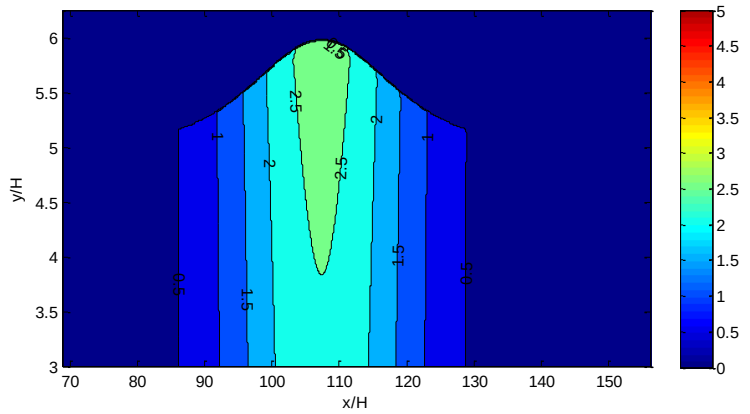

(b) u_0=0.0 m/s

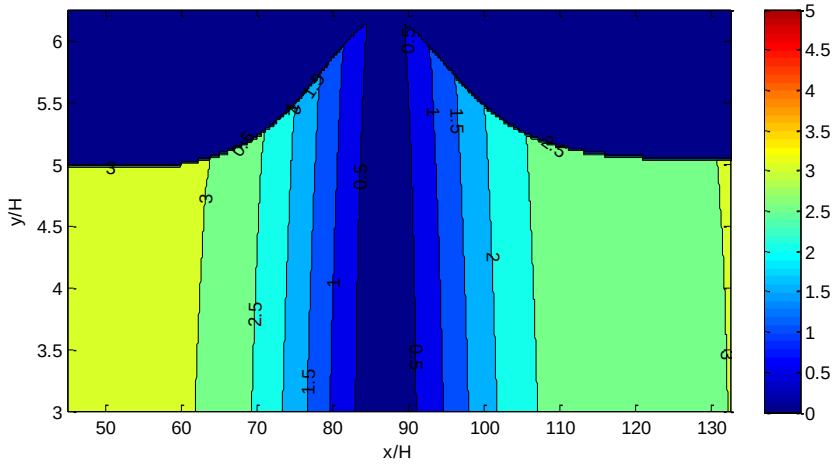

(c) u_0=-3.0 m/s

Figure 12 Effect of the current velocity on magnitude of the ensemble-averaged velocity (unit: m/s)

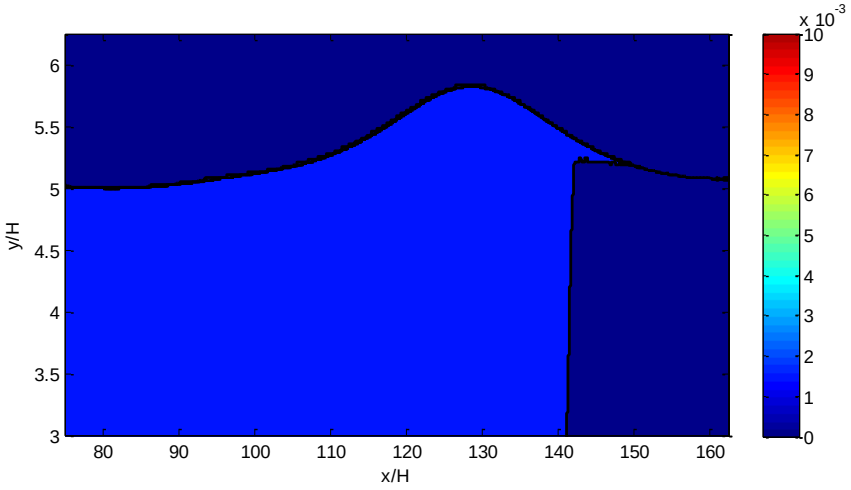

(a) u_0=3.0 m/s

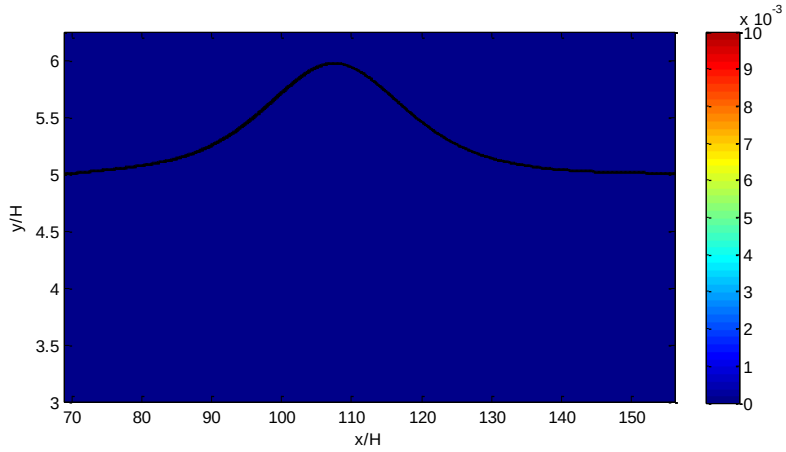

(b) u_0=0.0 m/s

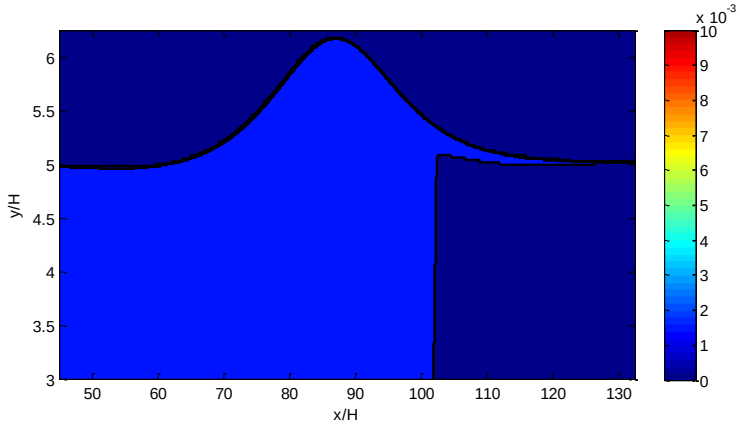

(c) u_0=-3.0 m/s

Figure 13 Effect of the current velocity on the turbulent kinetic energy (TKE, unit: m^2/s^2)